Hydrogel Micropillars with Integrin Selective Peptidomimetic Functionalized Nanopatterned Tops: A New Tool for the Measurement of Cell Traction Forces Transmitted through $\alpha_v\beta_3$- or $\alpha_5\beta_1$-Integrins

*Sabri Rahmouni, Aaron Lindner, Florian Rechenmacher, Stefanie Neubauer, Tariq Rashad Ali Sobahi, Horst Kessler, Elisabetta Ada Cavalcanti-Adam, and Joachim Pius Spatz**

Integrin-mediated adhesion plays a key role in mechanotransduction to the cytoskeleton by regulating signaling pathways that convey physical forces into chemical signals.[1,2] Several studies have focused on studying how the activation of specific integrin types and integrin receptor clustering may contribute to adhesion strength.[3–7] In particular, it has been reported that upon binding to fibronectin, $\alpha_v\beta_3$- and $\alpha_5\beta_1$-integrins have a distinct role in establishing adhesion. While $\alpha_5\beta_1$-integrin mediates adhesion strength, $\alpha_v\beta_3$-integrin is required for reinforcement and mechanotransduction.[8] Integrin clustering leads to the formation of focal adhesions, which are discrete structures where adherent cells establish contact to the extracellular matrix. Integrins bind to several signaling and structural proteins, thereby connecting the extracellular side of the membrane to the actin cytoskeleton.[9] Several proteins at focal adhesion sites mediate cellular responses to force; among these, zyxin is considered a key protein for mechanotransduction, since its localization at focal adhesions and along actin filaments is related to high contractility.[10,11]

S. Rahmouni, Dr. A. Lindner, Dr. E. A. Cavalcanti-Adam, Prof. J. P. Spatz
Department of New Materials and Biosystems
Max Planck Institute for Intelligent Systems
Heisenbergstr. 3, 70569 Stuttgart, Germany
E-mail: Spatz@is.mpg.de
S. Rahmouni, Dr. A. Lindner, Dr. E. A. Cavalcanti-Adam, Prof. J. P. Spatz
Department of Biophysical Chemistry
University of Heidelberg
Im Neuenheimer Feld 253, 69120 Heidelberg, Germany
Dr. F. Rechenmacher, Dr. S. Neubauer, Prof. H. Kessler
Institute for Advanced Study at the Department of Chemistry
Technische Universität München
Lichtenbergstr. 2a, 85748 Garching, Germany
Dr. T. R. A. Sobahi, Prof. H. Kessler
Chemistry Department
Faculty of Science, King Abdulaziz University
P.O. Box 80203, 21589 Jeddah, Saudi Arabia

DOI: 10.1002/adma.201301338

Two types of approaches have commonly been used in the last years to study forces in cellular systems: traction force microscopy and elastic micropillar systems.[12–18] Traction force microscopy analyzes the forces cells exert on plane substrates by tracking particles embedded in the elastic surface. It still remains a matter of debate how the actual forces are determined in detail, because the elastic matrix containing the particles couples to the lateral displacement of the matrix surface in a rather complex manner.[19] Micropillar systems provide a more direct measurement of forces. Each pillar has a known spring constant and can be examined independently; furthermore, the forces acting on a pillar can be correlated directly with the deformation of the pillar. Micropillars are typically made of polydimethylsiloxane (PDMS), which allows only a limited variation in the Young's modulus. The spring constant of the PDMS pillars ranges from 1,31 - 1556 nN/μm and is mainly adjusted by changing the pillar geometry, i.e. length and diameter.[20]

By choosing poly(ethylene glycol) diacrylate (PEG) over PDMS for micropillar fabrication we were also able to change the Young's modulus over a wide range (1 kPa to several MPa), while simultaneously benefiting from its protein repellent and cell adhesion suppressing properties.[21,22] The obtained PEG pillar presented a spring constant comparable to that of PDMS micropillars, but allowed to vary the spring constant by changing only the Young's modulus at a fixed pillar geometry. Inspired by reports on PEG micropatterning techniques, we established a fabrication method to obtain PEG micropillars applying microscope projection photolithography.[23,24] We were able to obtain aspect ratios of up to 10, center-to-center distances as low as 5 μm and diameters of 2 μm. Although more sophisticated methods to achieve PEG polymerization with submicrometer precision and to create 3-dimensional PEG structures exist, however, these methods require special devices for direct laser lithography.[25] In contrast, we used a fluorescence microscope with its HBO lamp as the illumination method of choice to achieve the formation of PEG structures. Overall, the aim was to keep the pillar size such that mature focal adhesions would fit on the pillar top, while reducing the Young's modulus.

The functionalization of pillar and traction force substrates is commonly realized by methods such as micro-contact-printing and incubation, which are based on the self-assembly of proteins or biologically active compounds of interest directly onto

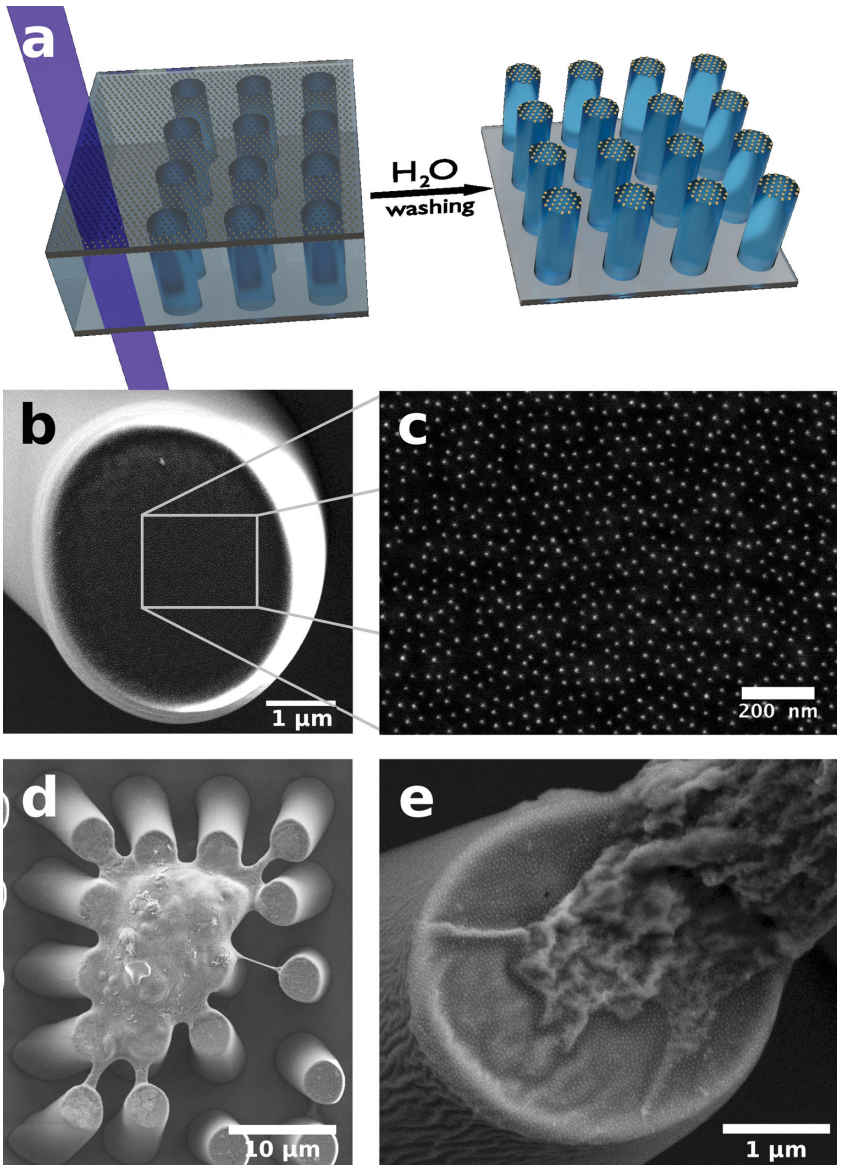

Figure 1. (a) The method for gold nanoparticle PEG pillar (GPPP) fabrication is illustrated. Left: illumination and polymerization of the fluid PEG using a UV ray; right: after rinsing with water and removal of the upper coverslip, the GPPP field stays on the lower silanized coverslip. SEM micrographs of (b) the top of a gold particle nano-patterened PEG pillar, (c) an enlarged image of the pillar top displaying the gold particle nanostructure, (d) a fixed REF-YFP-PAX cell on GPPPs and (e) close-up of a single pillar with an attached cell protrusion. Pillar bending in (d) is enhanced due to the fixation and drying process compared to live-cell experiments.

the substrate. A shortcoming of these methods is their inability to precisely control spacing and density of the presented functional molecules. To overcome these limitations we used surface nanopatterning, which permits the immobilization of molecules in a controlled manner. Sputtering and etching techniques, as well as block copolymer micellar nanolithography (BCML), are methods commonly used for surface nanopatterning.[26,27] Using BCML for the deposition of gold nanoparticles on hard surfaces, e.g. glass, has the advantage of being able to control both size (2–15 nm) and spacing (30–300 nm) of the gold nanoparticles. The gold particles can serve as an anchor for a whole variety of proteins and biologically active compounds which can be covalently bound via thiol linker molecules. Furthermore, it is possible to transfer the nanoparticles to biologically inactive PEG surfaces.[27] Here, we produced nanostructured micropillars by combining PEG micropillar fabrication with BCML gold nanostructures.

To fabricate gold nanoparticle structured PEG micropillars (GPPP), a layering approach (**Figure 1** (a)) was developed. In this regard, we stacked the following components in a sandwich-like structure: (i) an allyl-triethoxysilan-silanized glass slide as base, (ii) a 3–15 µl large drop of pre-polymer PEG solution (the volume depending on the desired length of the pillars to be constructed on the glass slide), and (iii) a coverslip with a gold nanoparticle pattern obtained by BCML and functionalized with a diacrylate linker on top. This arrangement was then placed on the specimen platform of the microscope. The samples were illuminated by UV light (360 nm) through the fluorescence pathway of an inverted microscope. As an illumination mask, a 100 µm pinhole was placed at the field-stop position within the fluorescent light path. Due to the limitations in platform positioning and shutter speed an illuminated spot accuracy of $\Delta t = 0.1$ s and $\Delta x = 1$ µm could be achived. Polymerization is initiated by illuminating the PEG pre-polymer solution with UV light, causing the PEG to covalently bind to both the silanized lower coverslip and to the gold nanoparticles located above *via* the attached linker. After rinsing with water and removal of the upper coverslip, the GPPP fields remained on the silanized coverslip.

A wide range of geometrically and physically different pillars could be produced by varying: (i) the pillar length by adjusting the amount of PEG between the coverslips, (ii) the focal length and magnification of the objective lens leading to pillars with diameters as small as 2 µm, (iii) the illumination time, (iv) the pattern defined by the input coordinates (e.g. rectangular, hexagonal, pairs), and (v) the molecular weight of the PEG pre-polymer solution. As a result, pillar spring constants can be adjusted to fit the experimental needs.

The spring constant of the PEG micropillars was determined using an AFM cantilever as a reference. First, the cantilevers spring constant was determined using the integrated tool of a JPK BioAFM (atomic force microscope, JPK Instruments AG). To calibrate the micropillars, the AFM cantilever was vertically fixed in a custom-made micromanipulator such that its tip was situated approximately 1 µm below the top of the PEG pillar. Both the cantilever and pillar were made to bend by moving

the microscope platform, and with it the pillar, towards the cantilever at a predefined constant velocity. This was monitored with a camera at a fixed frame rate. The acquired images were used to determine the position of the cantilever using the ICARUS video tracking software.[28] The PEG pillar spring constant was determined from the values of the cantilever spring constant, the stage speed and camera frame rate. In all cases the calibration curves show a linear relation for small deflections (< 5°), presenting a constant spring constant (Figure S1).

The smallest obtained spring constant was 0,35 ± 0,15 nN/µm. PEG pillars with even lower spring constants were produced, but could not be calibrated reliably by our cantilever method. In fact, a 10 nN/µm cantilever spring constant - the lowest we were able to monitor - caused only a minute, and therefore an imprecise tracking of the cantilever deflection. Stiffer pillars were fabricated by decreasing the pillar length or by using PEG with a lower molecular weight. For cell experiments the pillars were standardized to the following parameters: (i) 15 ± 2 nN/µm spring constant, (ii) 3.5 ± 0.5 µm diameter, (iii) 13 ± 1 µm length, and (iv) 8 ± 1 µm center-to-center spacing. With these settings the pillars were sufficiently elastic to be displaced up to 1,8 µm by the cells, but not too elastic to permit cell attachment. 55 ± 5 nm, an established ligand spacing for stable cell adhesion, was used as the spacing between gold nanoparticles (attached ligands).[29,30] The particle diameter was approx. 8 ± 2 nm.

The scanning electron microscope (SEM) images in Figure 1 (b) and (c) show the top of a PEG-pillar covered with gold nanoparticles. The nanoparticles are visible as bright dots with an approximate diameter of 8 nm.

We applied the nanostructured PEG micropillars as force sensors to assess the contribution of $\alpha_v\beta_3$- or $\alpha_5\beta_1$-integrins to cell traction forces.[6,8] To this end, $\alpha_v\beta_3$- or $\alpha_5\beta_1$-selective integrin antagonists were coupled to the gold nanoparticles on the pillar tops *via* thiol linkers (Figure S3).[31,32] Rat embryonic fibroblasts, which express both integrin types, were seeded on the PEG micropillars functionalized with either $\alpha_v\beta_3$- or $\alpha_5\beta_1$-integrin antagonists. SEM images show the adhesion of fibroblasts to the top surface of the functionalized PEG micropillars (Figure 1(d)).

To determine the impact of the recruitment of specific integrin-types at focal adhesion sites on cell forces, we monitored the displacement of the pillars upon cell adhesion. One hour after seeding, cells adhesion forces were monitored every 10 min by bright field and fluorescence microscopy over a period of 8 h. The acquired time-lapse images were analyzed to determine the maximum forces acting on each pillar within the observed time frame. Each pillar position was tracked and the maximum deflection during the time frame was determined. **Figure 2**(a) shows the forces generated by fibroblasts adhering to the two selective integrin-antagonists as the normalized frequency of the maximum forces observed on each pillar. Normalization was obtained by dividing each histogram bar by the total number of pillars used for this diagram. The histogram indicates that at approximately 7 nN the maximum force counts are comparable between cells on the $\alpha_v\beta_3$-integrin antagonist and cells on the $\alpha_5\beta_1$-integrin antagonist. For forces greater than 7 nN more counts are detected on the $\alpha_5\beta_1$-integrin antagonist. Figure 2(b) shows the difference between the data sets in percent, further

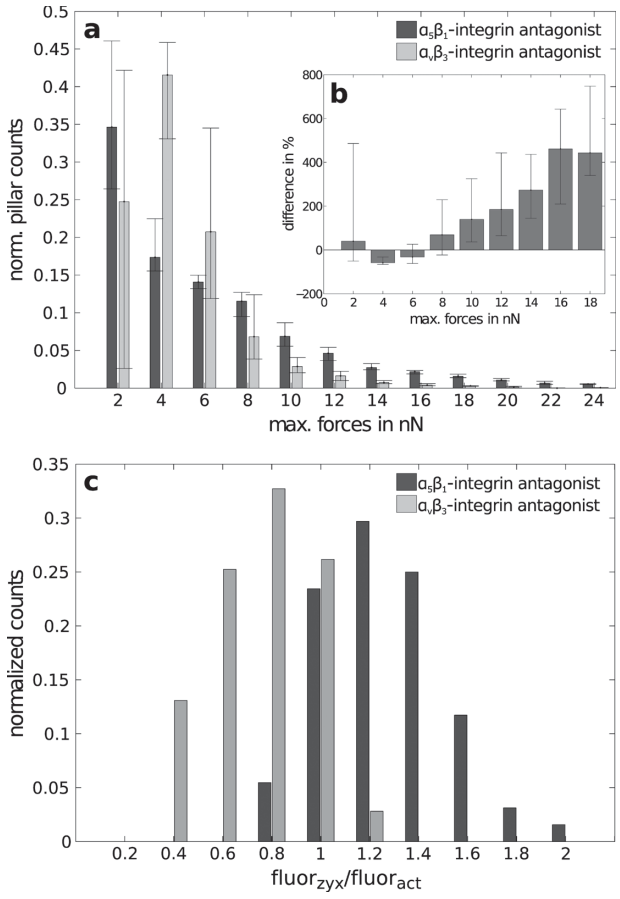

Figure 2. (a) Normalized frequency of the maximum cell traction forces observed on each pillar. The normalization was obtained by dividing each histogram bar by the total number of pillars analyzed for this diagram. (b) Plot of differences between $\alpha_5\beta_1$-integrin and $\alpha_v\beta_3$-integrin data sets shown in (a) in percent. (c) Normalized histogram of the zyxin by actin fluorescence intensity ratio on antagonist-bearing pillars that interact with the cell periphery (Figure 3). The ratio of the fluorescence intensity values directly reflects the ratio of zyxin protein to actin protein. In cells attached to the $\alpha_5\beta_1$-selective integrin antagonist the zyxin to actin fluorescence intensity ratio is higher than in cells attached to $\alpha_v\beta_3$-integrin antagonists. A two-tailed student's t-test reveals a significant difference between the two normal distributions with a p-value < 0.001.

highlighting the differences observed in Figure 2(a). The comparison in Figure 2(b) illustrates that for forces smaller than 7 nN only a few more maximum force counts are observed on the $\alpha_v\beta_3$-integrin antagonist than on the $\alpha_5\beta_1$-integrin antagonist. In contrast, at forces above 7 nN the number of maximum force counts on the $\alpha_5\beta_1$-integrin antagonist is up to four times greater than on the $\alpha_v\beta_3$-integrin antagonist. In general, the data shows a trend towards higher maximum force counts at higher force levels for cells on the $\alpha_5\beta_1$-integrin specific antagonist, suggesting that these cells must exert a greater pulling force on the pillars when adhering to them.

In separate experiments cells were fixed 5 h after seeding on the PEG micropillars and stained for actin, zyxin and paxillin. Focal adhesions (identified as paxillin clusters), were localized solely on the pillar tops (**Figure 3**). The fluorescence intensity

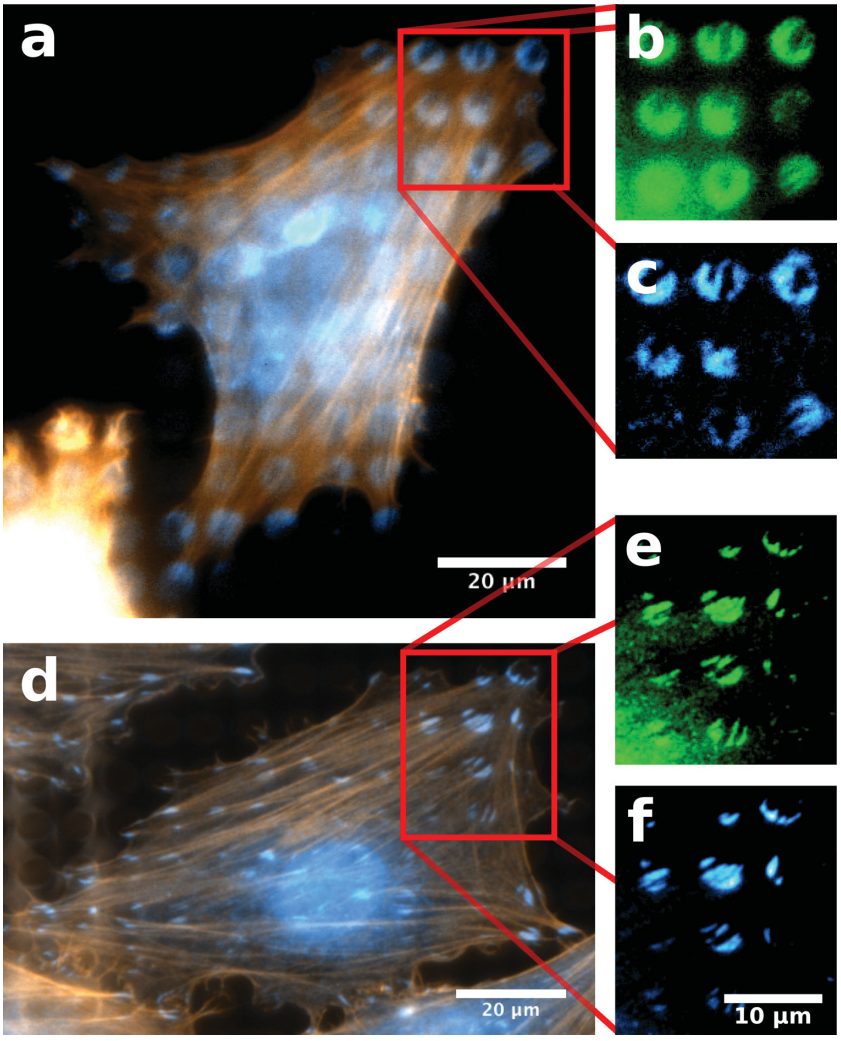

Figure 3. (a) Fluorescence image of fixed REF-YFP-PAX cells on GPPP decorated with ligands selective for $\alpha_v\beta_3$-integrins (a-c) or $\alpha_5\beta_1$-integrins (d-f). (a) and (d) show the actin network (orange) and zyxin (blue). (b), (c), (e), (f) show a magnified view of the cell areas framed by the red boxes. (b) and (e) show paxillin fluorescence (green, YFP); (c) and (f) show zyxin fluorescence (blue, CY5).

of zyxin and actin was monitored and quantified on several (n > 120) pillars connected to focal adhesions located at the cell periphery. To investigate differences in the focal adhesions formed by cells prior to cell fixation, we calculated the fluorescence intensity ratio of zyxin to actin (Figure 2(c)). On the $\alpha_5\beta_1$-integrin antagonist the ratio is much higher, indicating that more zyxin in relation to actin is present in the periphery of these cells compared to cells on the $\alpha_v\beta_3$-integrin antagonist. The significance was tested by a two-tailed student's t-test with a resulting p-value < 0.001 for the two normal distributions.

Our GPPPs proved to be a powerful tool for force measurements and cell adhesion manipulation. The advantages of this tool are as follows: 1) GPPP fabrication is simple and cost effective, 2) the GPPP spring constant and geometry can be easily varied and adjusted to experimentally required values, 3) the use of gold nanoparticle anchors for ligand binding allows control over the actual number of ligands per pillar top and ligand spacing, 4) covalent binding of a great variety of proteins and other biologically active compounds to the nanopatterned pillar tops is possible. Our fabrication method provides significant progress towards the production of highly versatile micropillars as we were able to produce a wide range of spring constants ranging from 0,35 - 100 nN/µm with pillar diameters as low as 2 µm and aspect ratios of up to 10. In this work, we used a spring constant of 15 ± 2 nN/µm a diameter of 3.5 ± 0.5 µm, a length of 13 ± 1 µm and a center-to-center distance of 8 ± 1 µm. We achieved biofunctionalization with two different peptidomimetics with high specificity for either $\alpha_5\beta_1$- or $\alpha_v\beta_3$-integrin. With this particular setup we were able to trace pillar bending and acquire reliable force data with a resolution as low as 0.7 nN.

We recently proved that the $\alpha_v\beta_3$- and $\alpha_5\beta_1$-integrin antagonists attached to gold nanostructured glass surfaces *via* a thiol group selectively bind their corresponding integrin.[31] In this study we functionalized GPPPs with either one of the two antagonists and monitored traction forces over time. To the best of our knowledge, this is the first study showing force measurements that can be attributed to specific integrin types at focal adhesion sites. Roca-Cusachs et al. measured the interaction of $\alpha_v\beta_3$- or $\alpha_5\beta_1$-integrins with either vitronectin or fibronectin-coated beads by magnetic tweezers, and reported that high forces are mainly mediated by $\alpha_5\beta_1$-integrins.[8]] They also describe that $\alpha_v\beta_3$-integrins initiate the reinforcement of integrin-cytoskeleton linkages through talin-dependent bonds. Our findings demonstrate that cells adhering *via* $\alpha_5\beta_1$-integrins exert higher maximum forces on the pillars than cells adhering *via* $\alpha_v\beta_3$-integrins. However, the fluorescence intensity ratio of zyxin to actin on the pillars attached to focal adhesions in the cell periphery shows higher zyxin levels on the $\alpha_5\beta_1$-integrin antagonist than on the $\alpha_v\beta_3$-integrin antagonist. This suggests that the mechanisms triggering adhesion and traction forces in close proximity to the cell edge may be different. Hence, integrin selective peptidomimetics anchored to nanostructured PEG micropillars provide a tool to further explore the molecular mechanisms underlying the recruitment of different integrins to adhesion sites.

In several studies it has been shown that forces localize at focal adhesions and that the focal adhesion size correlates with the amount of force that is applied. The amount of strain exerted on focal adhesions depends on substrate rigidity. Trichet et al. propose that the cytoskeleton dictates mechanosensing for cellular adaptation to substrate rigidity as part of a large-scale mechanism.[18] In agreement with this report, our findings on the range of overall maximum forces indicate

a similar maximum force exerted by cells that were seeded on pillars with a stiffness of approximately 15 nN/μm. Although a direct comparison of the measured values shows that the maximum deflection observed by Trichet et al. was 0.84 ± 0.03 μm, whereas we measured a maximum deflection of up to approx. 1.8 μm on both antagonists, this was only observed in very few instances. The mean deflection for the $\alpha_5\beta_1$-integrin antagonists and $\alpha_v\beta_3$-integrin antagonists obtained with our measurements is 0.43 ± 0.15 μm and 0.31 ± 0.14 μm, respectively. These values are comparable to those reported by Trichet et al.

These results, along with the findings on zyxin to actin ratios, indeed suggest that cytoskeletal organization may be pivotal in regulating the cellular mechanosensing response. Moreover, as the downstream pathways of $\alpha_5\beta_1$- and $\alpha_v\beta_3$-integrin signaling are quite distinct in terms of the recruited cytoplasmic proteins and cytoskeleton signaling, the amount of force at focal adhesions sites might be regulated by a feedback mechanism.[6] As a result, weaker cytoskeletal forces caused by physical or chemical properties of the substrate would lead to a decrease in force. This, in turn, would lead to a change in the localization of mechanosensor proteins. Our observation of a higher zyxin to actin ratio in cells attached to the $\alpha_5\beta_1$-integrin antagonist is in good agreement with this model. Zyxin localization correlates with the distribution of acting forces as previously reported.[33,34]

In conclusion, we developed highly versatile micropillars for measuring cell adhesion and traction forces. The pillars consist of poly(ethylene glycol) hydrogel and are nanopatterned with gold nanoparticles on the top surface. While the gold nanoparticles can be functionalized with different molecules, the hydrogel base of the pillars provides a protein-resistant interface, restricting unwanted interaction with biological material. Using this base material the bending stiffness of the pillars can be varied widely, ranging from less than 0.5 nN/μm to more than 100 nN/μm. At the same time, the size of the pillar top area is adjustable to fit mature focal adhesions. In our studies, the gold nanoparticles were functionalized with $\alpha_v\beta_3$- or $\alpha_5\beta_1$-integrin specific antagonists. This enabled the separate measurement of individual cellular traction forces, thus making possible to determine the contribution of different integrin-types to the total traction force. We demonstrate that cells binding to $\alpha_5\beta_1$-integrin antagonists have a tendency to exert higher maximum forces on the pillars than cells binding to $\alpha_v\beta_3$-integrin antagonists. These results are confirmed by staining experiments, which show a higher zyxin to actin ratio on the $\alpha_5\beta_1$-integrin antagonists at adhesion sites situated along the cell's outer edge. Future studies on the effects of different pillar properties and integrin ligand spacing will further elucidate the role of specific spatial cues in regulating cell mechanotransduction.

Experimental Section

Further information on the experimental materials and methods are available in the supporting information.

Supporting Information

Supporting Information is available from the Wiley Online Library or from the author.

Acknowledgements

We thank R. Fässler and J. Polleux for fruitful discussions. The support of the Max Planck Society is highly acknowledged. Part of the research leading to these results has received funding from the European Union Seventh Framework Programme (FP7/2007–2013) under grant agreement n° NMP4-LA-2009-229289 NanoII and n° NMP3-SL-2009-229294 NanoCARD. This work was funded by the National Institutes of Health (USA) through the Roadmap for Medical Research (PN2 EY016586). J. P. Spatz is the Weston Visiting Professor at the Weizmann Institute of Science. The group is part of the excellence cluster CellNetworks at the University of Heidelberg. S. Rahmouni thanks T. Haraszti for his experimentation and evaluation advices. F. Rechenmacher thanks the Bund der Freunde der TU München e.V. and IGSSE for financial support. S. Neubauer thanks CompInt of the elite network of Bavaria and the Max Planck Society for funding. H. Kessler acknowledges the financial support from King Abdulaziz University KAU (grant No. HiCi/25-3-1432).
Note: The license of this manuscript was updated after initial online publication.

Received: March 25, 2013
Revised: May 28, 2013
Published online: August 5, 2013

[1] S. Huang, D. E. Ingber, *Nat. Cell Biol.* **1999**, *1*, 131.
[2] M. A. Schwartz, R. K. Assoian, *J. Cell Sci.* **2001**, *114*, 2553.
[3] E. H. J. E. Danen, P. P. Sonneveld, C. C. Brakebusch, R. R. Fassler, A. A. Sonnenberg, *J Cell Biol.* **2002**, *159*, 1071.
[4] B. Geiger, J. P. Spatz, A. D. Bershadsky, *Nat. Rev. Mol. Cell Biol.* **2009**, *10*, 21.
[5] F. Li, S. D. Redick, H. P. Erickson, V. T. Moy, *Biophys. J.* **2003**, *84*, 1252.
[6] M. R. Morgan, A. Byron, M. J. Humphries, M. D. Bass, *IUBMB Life* **2009**, *61*, 731.
[7] C. Selhuber-Unkel, T. Erdmann, M. Lopez-García, H. Kessler, U. S. Schwarz, J. P. Spatz, *Biophysical Journal* **2010**, *98*, 543.
[8] P. Roca-Cusachs, N. C. Gauthier, A. Del Rio, M. P. Sheetz, *Proc. Natl. Acad. Sci. USA* **2009**, *106*, 16245.
[9] R. Zaidel-Bar, S. Itzkovitz, A. Ma'ayan, R. Iyengar, B. Geiger, *Nat Cell Biol.* **2007**, *9*, 858.
[10] R. R. Zaidel-Bar, C. C. Ballestrem, Z. Z. Kam, B. B. Geiger, *J Cell Sci* **2003**, *116*, 4605.
[11] P. J. Renfranz, M. C. Beckerle, *Curr Opin. Cell Biol.* **2002**, *14*, 88.
[12] K. A. K. Beningo, Y.-L. Y. Wang, *Trends Cell Biol.* **2002**, *12*, 79.
[13] J. J. Stricker, B. B. Sabass, U. S. U. Schwarz, M. L. M. Gardel, *CORD Conf. Proc.* **2010**, *22*, 194104.
[14] J. L. Tan, J. Tien, D. M. Pirone, D. S. Gray, K. Bhadriraju, C. S. Chen, *Proc. Natl. Acad. Sci. USA* **2003**, *100*, 1484.
[15] B. Li, L. Xie, Z. C. Starr, Z. Yang, J.-S. Lin, J. H.-C. Wang, *Cell Motil. Cytoskeleton* **2007**, *64*, 509.
[16] S. Ghassemi, G. Meacci, S. Liu, A. A. Gondarenko, A. Mathur, P. Roca-Cusachs, M. P. Sheetz, J. Hone, *Proc. Natl. Acad. Sci. USA* **2012**.
[17] O. du Roure, A. Saez, A. Buguin, R. H. Austin, P. Chavrier, P. Silberzan, P. Siberzan, B. Ladoux, *Proc. Natl. Acad. Sci. USA* **2005**, *102*, 2390.
[18] L. L. Trichet, J. J. Le Digabel, R. J. R. Hawkins, S. R. K. S. Vedula, M. M. Gupta, C. C. Ribrault, P. P. Hersen, R. R. Voituriez, B. B. Ladoux, *Proc. Natl. Acad. Sci. USA* **2012**, *109*, 6933.
[19] U. S. U. Schwarz, N. Q. N. Balaban, D. D. Riveline, A. A. Bershadsky, B. B. Geiger, S. A. S. Safran, *Biophys. J.* **2002**, *83*, 15.
[20] J. Fu, Y.-K. Wang, M. T. Yang, R. A. Desai, X. Yu, Z. Liu, C. S. Chen, *Nat. Methods* **2010**.
[21] J. Blümmel, N. Perschmann, D. Aydin, J. Drinjakovic, T. Surrey, M. López-García, H. Kessler, J. P. Spatz, *Biomaterials* **2007**, *28*, 4739.
[22] A. S. Hoffman, *Ann. New York Acad. Sci.* **2006**, *944*, 62.

[23] J. C. Love, D. B. Wolfe, H. O. Jacobs, G. M. Whitesides, *Langmuir* **2001**, *17*, 6005.
[24] A. Revzin, R. J. Russell, V. K. Yadavalli, W.-G. Koh, C. Deister, D. D. Hile, M. B. Mellott, M. V. Pishko, *Langmuir* **2001**, *17*, 5440.
[25] F. Klein, T. Striebel, J. Fischer, Z. Jiang, C. M. Franz, G. von Freymann, M. Wegener, M. Bastmeyer, *Adv. Mater.* **2010**, *22*, 868.
[26] M. M. Schvartzman, S. J. S. Wind, *Nano Lett.* **2009**, *9*, 3629.
[27] T. Lohmüller, D. Aydin, M. Schwieder, C. Morhard, I. Louban, C. Pacholski, J. P. Spatz, *Biointerphases* **2011**, *6*, MR1.
[28] S. Gibson, R. J. Hubbold, J. Cook, T. L. J. Howard, *Comput. Graphics* **2003**, *27*, 293.
[29] M. Arnold, E. A. Cavalcanti-Adam, R. Glass, J. Blümmel, W. Eck, M. Kantlehner, H. Kessler, J. P. Spatz, *ChemPhysChem* **2004**, *5*, 383.
[30] E. A. Cavalcanti-Adam, T. Volberg, A. Micoulet, H. Kessler, B. Geiger, J. P. Spatz, *Biophys. J.* **2007**, *92*, 2964.
[31] F. Rechenmacher, S. Neubauer, J. Polleux, C. Mas-Moruno, M. De Simone, E. A. Cavalcanti-Adam, J. P. Spatz, R. Fässler, H. Kessler, *Angew. Chem. Int. Ed.* **2013**, *52*, 1572.
[32] F. Rechenmacher, S. Neubauer, C. Mas-Moruno, P. M. Dorfner, J. Polleux, J. Guasch, B. Conings, H. Boyen, A. Bochen, T. R. Sobahi, R. Burgkart, J. P. Spatz, R. Fässler, H. Kessler, *Chem. Eur. J.* **2013** DOI: 10.1002/chem.201301478
[33] D. A. D. Nix, J. J. Fradelizi, S. S. Bockholt, B. B. Menichi, D. D. Louvard, E. E. Friederich, M. C. M. Beckerle, *J. Biol. Chem.* **2001**, *276*, 34759.
[34] M. M. Yoshigi, L. M. L. Hoffman, C. C. C. Jensen, H. J. H. Yost, M. C. M. Beckerle, *J. Cell Biol.*. **2005**, *171*, 209.
[35] J. Schindelin, I. Arganda-Carreras, E. Frise, V. Kaynig, M. Longair, T. Pietzsch, S. Preibisch, C. Rueden, S. Saalfeld, B. Schmid, J.-Y. Tinevez, D. J. White, V. Hartenstein, K. Eliceiri, P. Tomancak, A. Cardona, *Nat. Methods* **2012**, *9*, 676.
[36] I. F. Sbalzarini, P. Koumoutsakos, *J. Struct. Biol.* **2005**, *151*, 182.